Atmospheric Research 273 (2022) 106182

Contents lists available at ScienceDirect

Atmospheric Research

journal homepage: www.elsevier.com/locate/atmosres

Demonstrating the asymmetry of the Indian Ocean Dipole response in regional earth system model of CORDEX-SA

Alok Kumar Mishra [a], Pankaj Kumar [a,*], Aditya Kumar Dubey [a], Sanjeev Kumar Jha [a], Dmitry V. Sein [b,c], William Cabos [d]

[a] Department of Earth and Environmental Sciences, Indian Institute of Science Education and Research Bhopal, India
[b] Alfred Wegener Institute for Polar and Marine Research, Bremerhaven, Germany
[c] Shirshov Institute of Oceanology, RAS, Moscow, Russia
[d] University of Alcala; Alcala, Spain

ARTICLE INFO

Keywords:
IOD
Atmosphere-Ocean interaction
RESM
CORDEX-SA

ABSTRACT

An accurate representation of the Indian Ocean Dipole (IOD) is crucial for the reliable projection of Indian summer monsoon rainfall, making it necessary to improve the understanding of the response of the IOD in the warming climate. For the first time, a high-resolution regional earth system model (RESM) over the CORDEX-SA domain is used to investigate the IOD characteristics. The model performance is evaluated in simulating the IOD and associated mechanism. RESM shows a good resemblance in simulating IOD phases (positive and negative). However, the systematic discrepancy is observed in magnitude. Additionally, RESM well represented the positive IOD's inter-event variability. For example, the stronger event dominated by significant cold anomalies over Sumatra with enhanced westward-extended while a moderate event shows weak cooling confined to the region of Sumatra. Additionally, RESM shows potential to distinguish the ENSO and non-ENSO years with more remarkable skill in representing the spatial pattern of SST over IOD region during non-ESNO years than ENSO years. The RESM realistically simulated the IOD amplitude with greater skill than CMIP5/6 models reported in the earlier studies, indicating reliability towards the projection of the Indian summer monsoon. The weaker IOD-ENSO relationship is caused by producing the more significant number of IOD during non-ENSO years. Despite this reliable fidelity, IOD's slightly earlier peak is driven by the early establishment of low-level equatorial easterly wind. This study provided valuable insight into the IOD's different phases, responsible forcings, and limitations of the RESM in accounting for the role of internal climate variability that can be useful for further improvement in the model physics.

1. Introduction

The Indian Ocean Dipole (IOD) represents the most prominent mode of interannual variability in the tropical Indian Ocean (Saji et al., 1999). It starts developing in May and attains its peaks in fall (September–October-November; SON) and decay in winter (December–January-February; DJF) with strong year-to-year variability. IOD profoundly impacts the strength of seasonal Indian summer monsoon rainfall (ISMR) and its variability (Ashok and Saji, 2007; Hrudya et al., 2021). The number of IOD events is projected to increase in a warming climate, particularly the number of intense positive IOD events (Cai et al., 2021, 2014).

The IOD is measured by the index called the Diople mode index (DMI). A positive IOD (pIOD) deals with warm sea surface temperature (SST) anomalies in the equatorial western Indian Ocean and cold anomalies in the east and vice versa for the negative IOD (nIOD). IOD variability profoundly impacts the local climate and the ISMR. Its influences the large-scale ocean-atmosphere circulations further impact weather extremes in Indian Ocean-rim countries (Ashok et al., 2003; Cai et al., 2009; Saji et al., 1999) such as droughts, floods, heatwaves, and bushfires, marine hazards, destruction of ecosystems, fishery, and coral reef death. Additionally, it affects the climate of various parts of the globe through atmospheric teleconnection (Saji and Yamagata, 2003; Saji et al., 1999). It's positive(negative) phase brings wetter(drier) than normal over India. However, the negative phase's impacts are generally lesser than the positive phase (Ashok et al., 2001). These significant

* Corresponding author at: Department of Earth and Environmental Sciences, Indian Institute of Science Education and Research Bhopal, Bhopal 462066, India.
E-mail address: kumarp@iiserb.ac.in (P. Kumar).

https://doi.org/10.1016/j.atmosres.2022.106182
Received 5 October 2021; Received in revised form 21 March 2022; Accepted 5 April 2022
Available online 9 April 2022

impacts highlight the necessity of an accurate representation of the IOD and its interaction with other climate modes in climate models to investigate the future change in the Indian ocean and IOD in a warming climate. For instance, a recent study by Cai et al. (2021) reported a decrease(increase) in moderate(intense) pIOD events in a warmer climate and suggested a contrast mechanism associated with these events. The reliability of this projection relies on the model's potential in reproducing the IOD and associated mechanisms that can enhance the predictability of ISMR.

In the last decade, several researchers have looked into the IOD variability and associated mechanism (Ashok et al., 2001; Ashok and Saji, 2007; Cai et al., 2021; Pokhrel et al., 2012). The Indian ocean dynamics govern the IOD (Vinayachandran et al., 2002), which is regulated by the combination of internal processes in the Indian Ocean (Bjerknes feedback, surface, and subsurface oceanic properties, zonal SST gradient, wind stress, thermocline depth, and upwelling). Besides, it is subject to remote influences such as ENSO (El Niño Southern Oscillation), which triggers and modulates its evolution (Fan et al., 2017; Hong et al., 2008; Sun et al., 2015). These complex features and their linkage with various local dynamical and thermodynamical processes and remote teleconnection make modeling the IOD challenging (Cai and Cowan, 2013). The impacts, as mentioned above, of IOD on climate variability highlight the importance of realistic simulation of these components for the reliable projection of climate over IOD influencing regions.

The relation of various climate modes, including IOD and ENSO, with ISMR, are getting changed in the warming climate. Earlier studies are reported the weakening(strengthening) relation of ENSO(IOD) with ISMR, which may affect the performance of statistical models used for ISMR prediction. A study by Wang et al. (2015)) reported the decreased performance of the statistical model used in the operational forecast for ISMR in the recent era (2000−2010) compared to the precedence decades. Thus understanding, how the IOD responds to a warmer climate is of the utmost importance.

The global climate models (GCMs) are used in global warming projections. However, they pose substantial uncertainty in simulating the structure of IOD and its relation to ENSO, reducing the reliability of their projections. For instance, the mesoscale eddies over the Indian ocean influence heat transport away from the eddies location and vertically at the location, hence developing and decaying IOD. Thus high-resolution coupling is demandable to increase the model's performance. However, the considerable computation cost of high-resolution simulations with GCMs limits their use. Alternatively, the regional atmosphere-ocean coupled model or regional earth system model (RESM) can be used at an optimum computational cost (Di Sante et al., 2019; Mishra et al., 2021a). The main objective of this study is to implement a new high-resolution RESM, namely ROM(Sein et al., 2015), over the CORDEX-SA region and evaluate the model's capability in simulating the IOD.

2. Model, methodology and data set used

2.1. Model setup

The RESM used in this study consists of a global ocean model namely

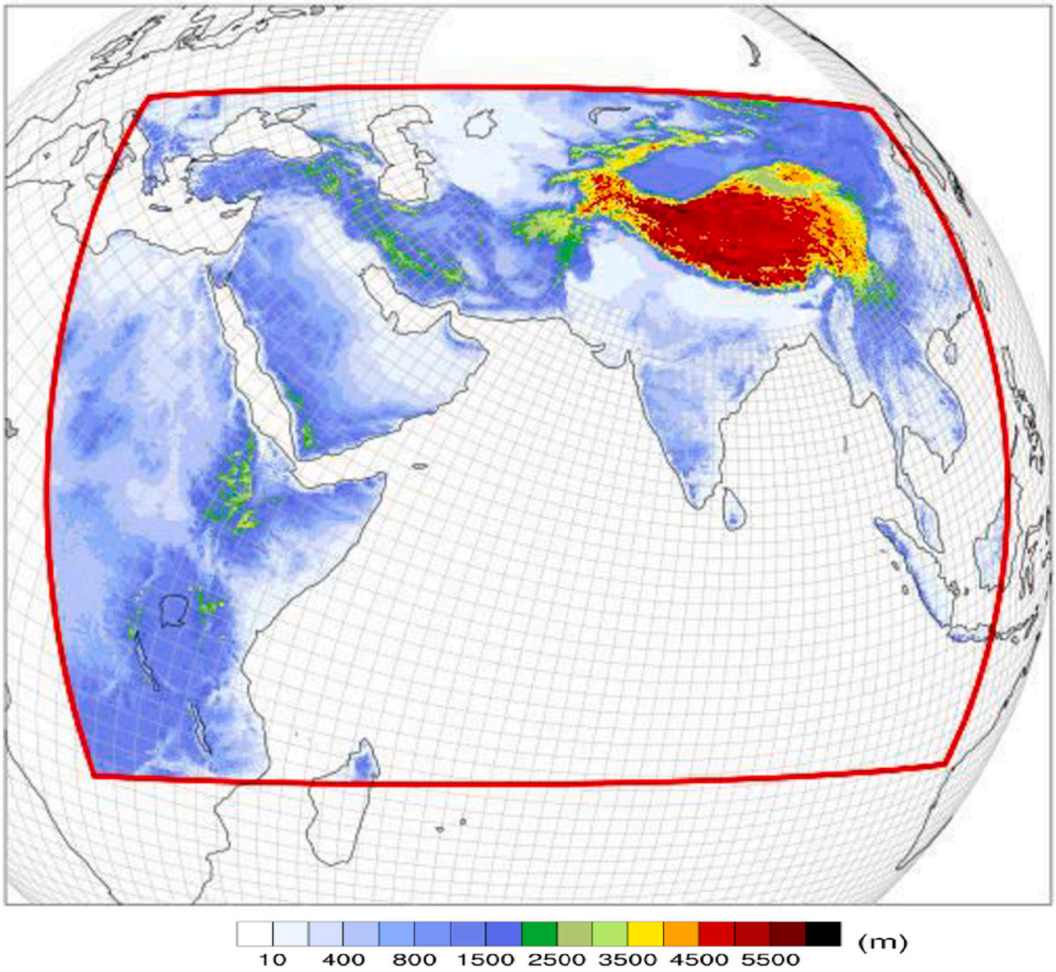

Fig. 1. Model domain and topography (a). Red Box shows the region where the Ocean model is coupled with the atmospheric model. (For interpretation of the references to colour in this figure legend, the reader is referred to the web version of this article.)

Max Planck Institute Ocean Model (MPIOM) (Jungclaus et al., 2013), a limited-area Regional Model (REMO) (REMO, Jacob, 2001) as an atmospheric component, and a Hydrological Discharge model (HD) (Hagemann and Dümenil, 1998) that provides the continental runoff to the ocean model and delivers freshwater discharge at the exact river mouth. The atmosphere-ocean coupling is performed over the coordinated regional downscaling experiments (CORDEX) for South Asia (CORDEX-SA) (Giorgi et al., 2009) (Fig. 1). A detailed description of the model setup can be found in Sein et al. (2015, 2020) and (Mishra et al., 2021b).

MPIOM is formulated with the hydrostatic approximation covering the global domain, which makes it different from the conventional regional earth system models (generally use regionally configured ocean model) that rely on information provided by the global ocean model at the lateral boundaries (LB) creating several issues (Sein et al., 2020, 2015). For example, (i) inconsistencies between the regional model solution and the LB data due to differences in resolution or physics of LB source (ii) uncertainty on the influence of coastal waves originating from outside the target region (beyond coupled domain consisting regional ocean model). The global ocean model overcomes these complications, which brings important advantages for climate change scenario simulations. For instance, it allows for the investigation of possible long-term changes in some oceanic extreme events, which are generally not possible in regional ocean models due to the use of monthly mean data as a lateral boundary condition. MPIOM employed a varying horizontal resolution having higher resolution over the target region of study (Indian Ocean). Over the open Ocean of the Indian Ocean, horizontal resolution is taken as ~20 km, which further increased up to 10 km (eddy-permitting) over the coastal region and decreased gradually, reaching a minimum of 100 km in the southern seas. We use 40 unevenly spaced vertical z-levels. The model is also equipped with tidal forcing, derived from the full ephemerides lunisolar tidal potential (Thomas et al., 2001). The MPIOM uses bottom boundary layer slope convection (Marsland et al., 2002) and an isopycnal diffusion scheme (Griffies, 1998). Since, MPIOM is integrated globally, no lateral boundary is required, however, it is initialized with Polar Science Center Hydrographic Climatology (PHC) (Steele et al., 2001)) and ran in the spin-up mode for 90 years cyclically with ERA-40 reanalysis forcing (2 times for 45 years, from 1958 to 2002). The atmospheric fields (10 m zonal and meridional wind, 2 m air temperature, dew point temperature, downward short wave, and longwave radiations, total precipitation) obtained from the ECMWF ERA-Interim (EIN) reanalysis (Dee et al., 2011) are prescribed as external atmospheric forcing outside the coupled domain. Using these fields, MPIOM computes heat, freshwater, and momentum fluxes following Marsland et al. (2002).

REMO is integrated at a horizontal resolution of 0.22° (~25 km) in the rotated grid and 27 hybrid vertical levels which is regionally configured over CORDEX-South Asia. All model components are coupled via the OASIS coupler (Valcke, 2013) with a coupling frequency of 3 h (coupled time step) for the atmosphere and ocean that realistically represent the diurnal cycle. The high coupling frequency and the inclusion of tidal dynamics led to correct resolving the regional high-frequency interaction that was neglected in most of the GCMs. The six-hourly varying lateral boundary conditions for REMO are obtained from EIN. These boundary fields are relaxed in the outer eight grids (buffer zone is excluded from the analysis) of the model following the method of (Davies, 1976). The fractional land surface scheme is adopted for the land-surface process (Rechid et al., 2009). The stand-alone REMO (i.e., without oceanic model coupling) is prescribed with National Oceanic and Atmospheric Administration (NOAA) Optimum Interpolation (OI) SST (Reynolds et al., 2007).

The model results are stored for 38 years from 1 January 1980 to 31 December 2017 after removing the initial transients (spinup).

2.2. Methodology

The different climatological baselines in the earlier studies led to variation in classification and number of IOD events. Also, the strong warming trend in the equatorial Indian Ocean put challenges to correct the selection of baseline. These problems could be overcome using the longest possible period (data set availability period) to calculate the climate normal (Ummenhofer et al., 2009; Verdon and Franks, 2005). Thus in this study, the SST anomalies for the peak phase of IOD (September–October-November: SON) are computed by subtracting the mean SON climatology for 1980–2017. Besides, a linear trend is removed before computing the empirical orthogonal function (EOF) and DMI. The detrending ensures the modes are not due to the trend in the data. The east pole (10°S–0°,90°–110°E, hereafter IODE) and west pole (10°–10°N, 50°–70°E, hereafter IODW) boxes used in this study are the same as (Saji et al., 1999). The difference between SST over IODW and IODE represents DMI. Based on the DMI, the year having greater than ± one standard deviation (SD) during the peak phase of IOD (SON) is considered as the positive/negative IOD years, which are consistent with earlier studies (Rao et al., 2002; Verdon-Kidd, 2018). Apart from this, the positive IOD years are further categorized into strong and moderate, with strong years having greater than 1.5 SD and composites computed for all IOD categories. The positive IOD years, 1982, 1987,1997, 2006, 2015, the negative IOD years 1981, 1992, 1996,1998, 2000, 2005, 2016 are considered for calculating the composite of positive and negative IOD years. The year 1994 is considered as the asymmetric positive IOD (apIOD) years.

2.3. Observational data sets

To compare with model simulations, we used the Hadley Centre Sea Ice and Sea Surface Temperature data set (HadISST; Rayner et al., 2003). We also used subsurface ocean data (Temperature, Zonal and meridional velocity, the thermocline depths, defined by the depth of 20 °C isotherms) from the European Centre for Medium-Range Weather Forecasts Ocean Reanalysis System 5 (ECMWF ORAS5; Zuo et al., 2019). The high resolution (~ 10 km horizontal resolution) precipitation derived from MSWEP (Beck et al., 2019) is used to demonstrate the ROM's potential in simulating precipitation IOD patterns and zonal and meridional wind obtained from an advanced reanalysis product of ECMWF; the ERA5 (Mahto and Mishra, 2019).

3. Results

This study demonstrated the capabilities of the ROM in simulating the IOD and associated mechanisms.

3.1. ROM's evaluation for IOD

An empirical orthogonal functions(EOF) analysis is performed on the monthly SST to characterize the inter-annual variability of the IOD. Fig. 2 shows the two leading modes of EOF patterns from the ROM and corresponding observation. The first EOF shows the positive anomaly over western TIO, including the Arabian Sea, and negative anomaly eastern TIO along Sumatra. Similarly, the second EOF shows the positive anomaly along Sumatra and a negative anomaly over western TIO. ROM bears a good resemblance to the observed pattern, however, the magnitude of anomalies are slightly overestimated/underestimated, particularly in the eastern tropical Indian Ocean. The negative anomaly is slightly stronger and confined to a narrow region along the eastern coast in the first EOF. In contrast, the positive anomaly is confined to Sumatra rather than the westward extended up to the equatorial region in the observation. Additionally, ROM correctly follows the temporal evolution of PC1 and PC2. The pattern correlation coefficient between the ROM and observed IOD for the first and 2nd modes is 0.82 and 0.74.

To demonstrate the model skill in representing IODs, we represent in

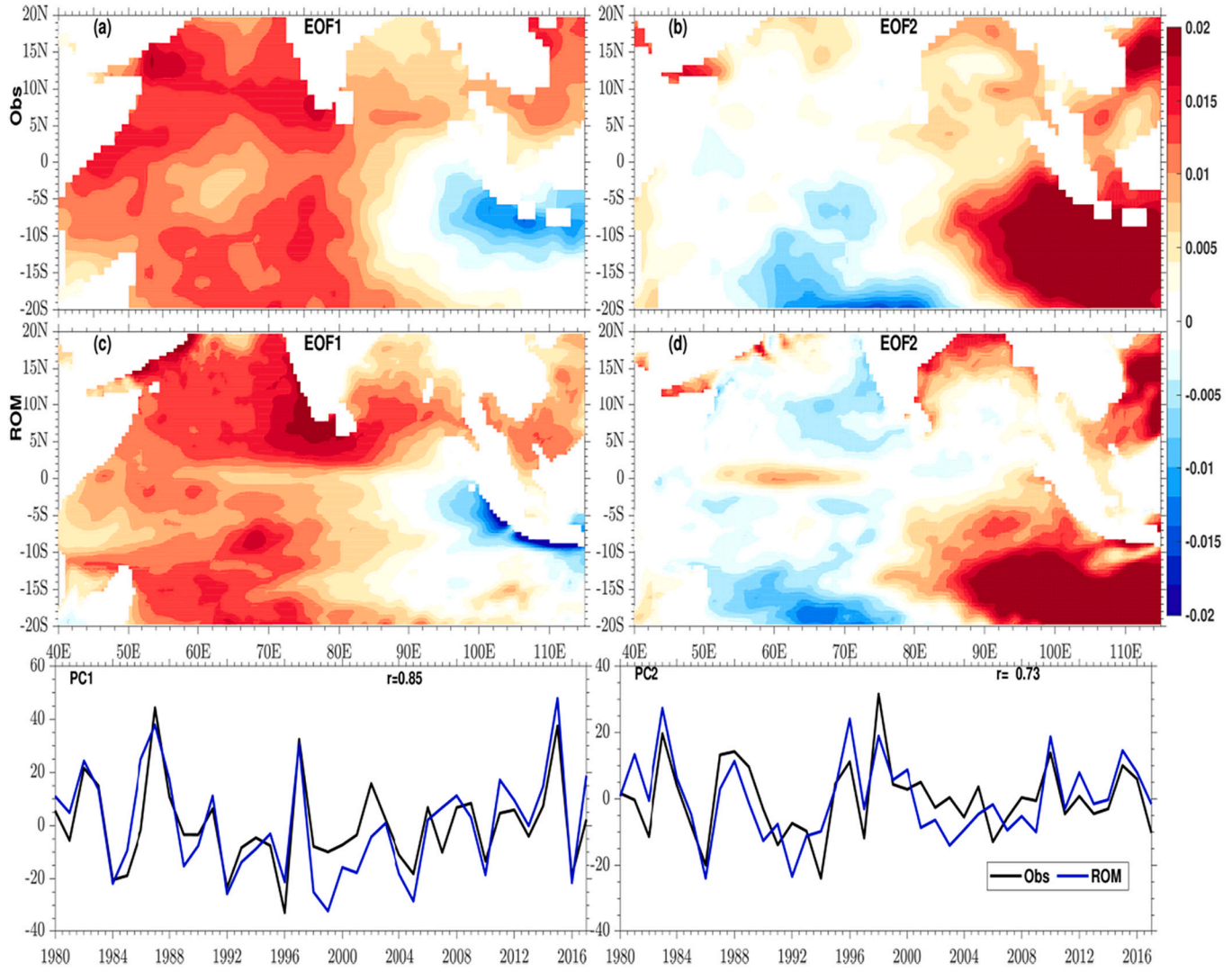

Fig. 2. Two leading modes of SST EOF and its principal components for ROM and observation The black solid line is for observation, and blue is for the model. (For interpretation of the references to colour in this figure legend, the reader is referred to the web version of this article.)

Fig. 3 the time series of the yearly peak phases (positive and negative) of simulated DMI with corresponding observation. It is observed that the magnitude of most of the warm events exceeds the magnitude of the cold events, illustrating the IOD asymmetry. SSTA of the eastern pole shows a more potent cold (−0.68 °C) anomaly than the warm (0.48 °C) anomaly, whereas the western pole shows a more robust warm (0.68 °C) anomaly than cold events (Fig. S1). The net effect of the two-pole DMI tends to show a more prominent asymmetry skewed towards the positive anomaly. ROM shows good skill in simulating in representing most of IOD events and overall positive skewness. These results are consistent with the previous study of (Hong et al., 2008). The observed pIODs in 1994, 1997, 2006, 2011, 2015 are reproduced by the model. However, the model produces some unrealistic pIODs that are either absent or too weak in observation. Similarly, ROM potentiality reproduces the nIOD events and their weakening in the recent era slightly overestimated magnitude. The correlation coefficient (CC) between ROM and observed DMI, IODE and IODW are 0.75, 0.73, and 0.68. These CC's are significant at a 99.9% significance level.

To boost up the confidence in the modeled results, we make a comparative investigation of dipole mode index (DMI) for ROM and CMIP6 with observation to verify the improvements. In this regard, we computed the IOD-A for the ROM and CMIP6 models (Fig. S2) during the peak phase of the IOD. The time period of this comparison is (1980–2014) common to all models and observation, which is slightly different than the study period (1980–2017) but subjected to the availability of CMIP6 historical data up to 2014. From the figure, it can be noticed that most of the CMIP6 model shows large discrepancy in reproducing the DMI. ROM shows comparatively lesser bias than the CMIP6 model.

The skewness, a measure to quantify the asymmetry, is computed for DMI along with its east-west pole, shown in Table 1. These values are significant at 99.9%. SST variability is found to be negatively(positively) skewed over the eastern(western) pole with greater skewness over the western pole, making the DMI skewness positive. Hong et al. (2008) emphasized the importance of asymmetric thermocline-SST feedback, wind–evaporation–SST for skewness, and asymmetry in IOD amplitude. Further investigation on the physical reasons behind the remained amplitude bias in ROM would be interesting but is beyond the scope of this study.

The IOD amplitude (IOD-A), which is defined as the standard deviation DMI has a large implication on the model's reliability as the bias in the IOD-A in the present climate day model can affect the climate projections (Cai and Cowan, 2013). Thus, it is worthwhile to investigate the model's potential in representing IOD-A. Fig. 4 reveals strong seasonality of IOD amplitude, with the minimum in winter and peaking during SON in the observation. ROM follows more or less a similar pattern of

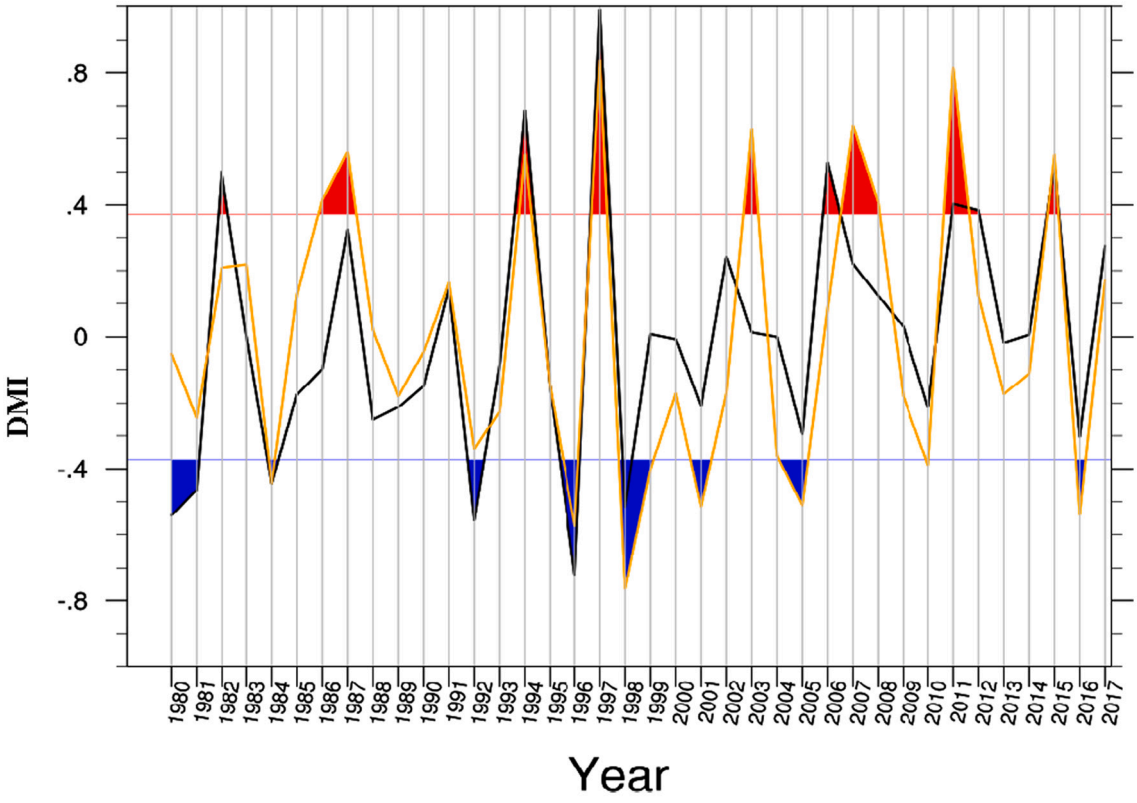

Fig. 3. Dipole mode Index (DMI) for ROM (yellow solid line) and observation (black solid line). Blue shaded represents the negative IOD years, and red shaded represents the positive IOD years.

Table 1
Skewness of IODE, IODW, and DMI index for ROM and observation.

Index	Skewness			
	Monthly		SON	
	Observation	ROM	Observation	ROM
DMI	0.31	0.25	0.41	0.35
IODE	−0.11	−0.33	−0.86	−0.63
IODW	0.41	0.34	0.05	0.26

temporal evolution with a systematic discrepancy of overestimation and early peaking. The IOD amplitude overestimation is a pervasive problem in most CMIP5/6 models reported in earlier studies (Cai and Cowan, 2013; McKenna et al., 2020). This bias is substantially lesser than the bias in the ensemble mean CMIP5 and CMIP6 model that shows 1.8 times larger amplitude than observation (Cai et al., 2013). Cai and Cowan (2013) reported the shallow thermocline and stronger SST over the eastern equatorial Indian ocean (EEIO). Their study also reported the thermocline feedback as common biases in most models with large-amplitude bias. We also observed large asymmetry in the IOD eastern pole and western pole). In general the stronger of warm phase is noticed over the western pole than the respective colder phase over eastern pole. Thus the model having larger IOD amplitude systematically produces weaker(stronger) warming over eastern(western) tropical IO with unrealistically more remarkable future rainfall changes. We also make a comparative investigation of IOD-A with models of CMIP6 to verify the improvements. In this regard, we computed the IOD-A for the ROM and CMIP6 models (Fig. S3) during 1980–2014 for the peak phase of the IOD. This time period is slightly different than the study period (1980–2017) but subjected to the availability of CMIP6 historical data up to 2014. From the figure, it can be noticed that most of the CMIP6 model shows the large spread in reproducing the IOD-A, with massive overestimation that varies with months and models. The model with a minimum(maximum) bias in the CMIP6 model shows nearly 1–5 and ~ 4 times larger amplitude than observation. ROM shows comparatively lesser bias than the CMIP6 model. The reduction of IOD amplitude in our model setup enhanced the reliability of future projection Indian summer monsoon.

Further, an effort is made to investigate the model's potential in simulating the spatiotemporal distribution of anomalously warm and cold ocean states during the peak phase of IOD. In this regard, we have computed the composite of SSTA for nIOD, pIOD, and asymmetric IOD (apIOD) (Sun et al., 2014) years (Fig. 5) that reveals contrasting SST anomaly patterns in the eastern and western poles, indicating dipole-like structures that alternatively changes in the positive and negative phase. For example, positive and negative anomalies over the eastern and western pole during negative years and vice-versa during positive phase. ROM bears a close resemblance with observation for the distinct distribution of SST during the warm and cold phases of IOD. Earlier studies have reported that the symmetric and asymmetric IOD years have very different SST distribution and affect the ISMR (Cai et al., 2013; Crétat et al., 2017). The year 1994 was reported as an asymmetric IOD year that shows different anomaly patterns rather than the traditional IOD one. ROM correctly reproduces the SSTA distribution for the different phases of IOD, particularly for apIOD of 1994 that makes its successful predictive skill of ISMR precipitation during 1994 (fig. S4) as most of the other models fail to predict the ISMR year 1994. However, the cold SST anomalies (and hence dry anomaly) are confined to the western equatorial Indian Ocean due to the weaker southeasterly over Sumatra. Besides, ROM shows easterly wind over the equatorial region from the eastern to western coast rather than convergent flow over the central equatorial IO as in observation, indicating a model deficiency in simulating the IO climate.

We showed the inter-events variation of pIOD (Fig. 6). The pIOD shows a strong asymmetry in the warm and cold area spread and

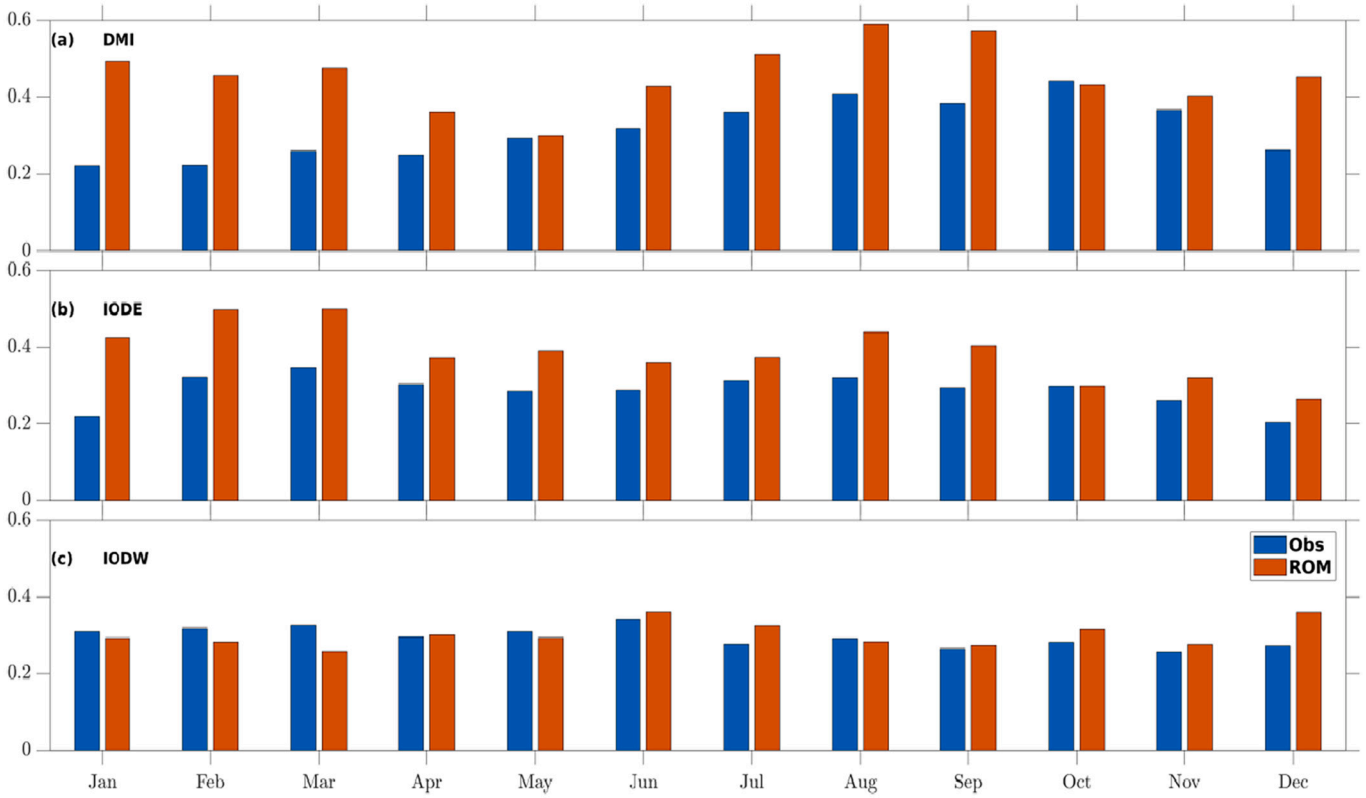

Fig. 4. IOD amplitude (standard deviation) for (a) DMI (b) Eastern pole (c) western pole.

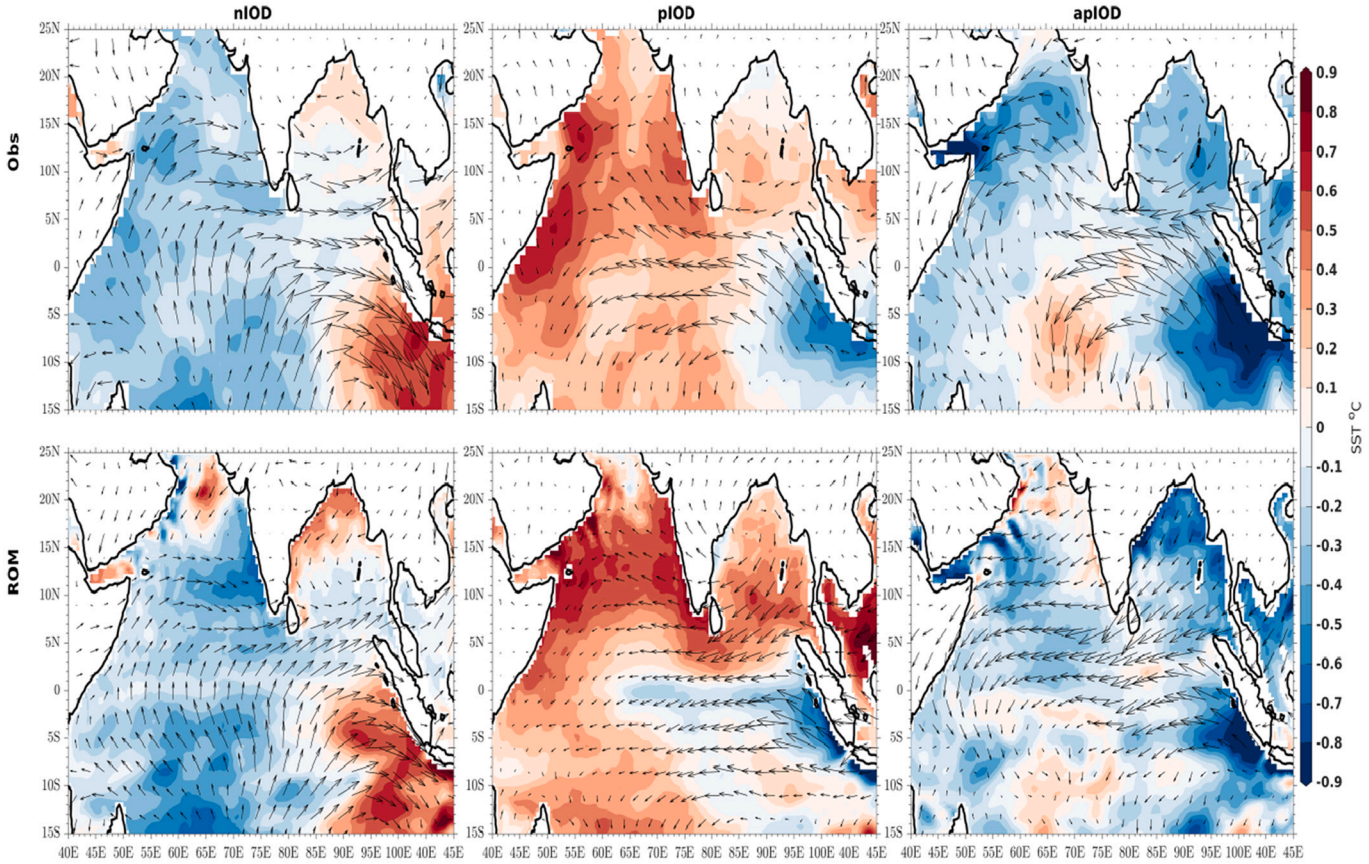

Fig. 5. Composite of SST anomalies (^{0}C, shaded) and low-level wind (m/s, vector) for nIOD, pIOD, and apIOD.

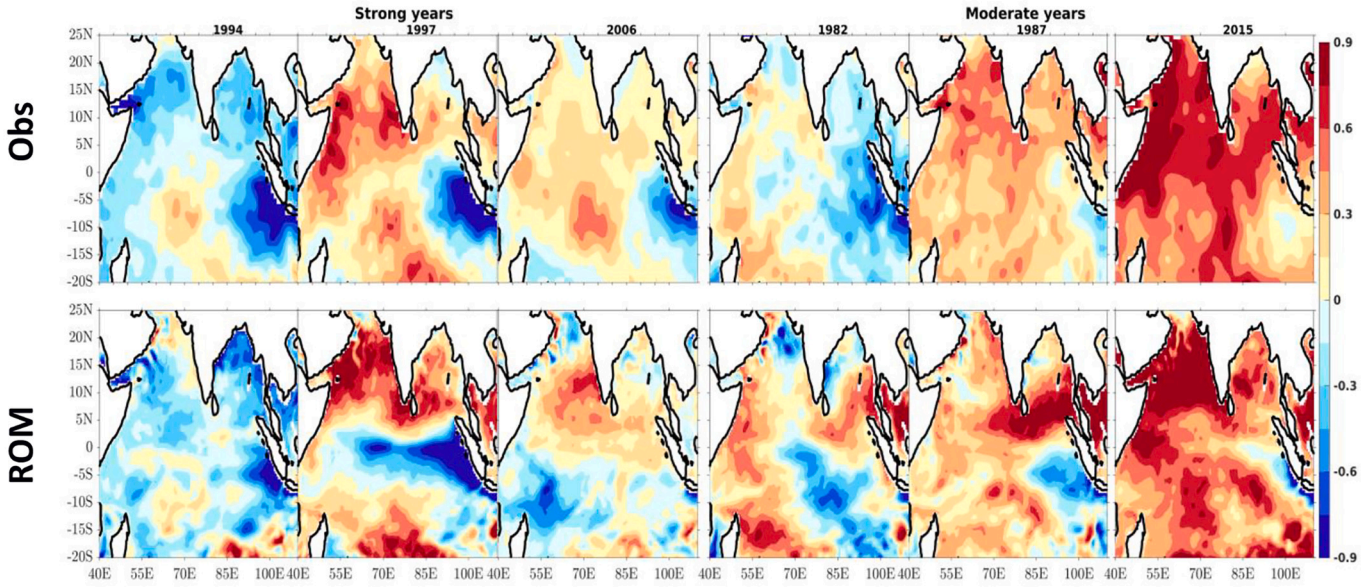

Fig. 6. Composite of SST anomaly for the different positive IOD years (Strong and Moderate) during 1980–2017.

magnitude ranging from an extreme event dominated by the stronger and westward extension of cold anomalies to a moderate event with weaker cooling confined to the region off Sumatra-Java. Interestingly all IOD events are not found to display the conventional dipole signature pattern of warming and cooling at opposite poles, as reported in the pioneer study by Saji and Yamagata (2003). It is important to note that a substantial positive or negative DMI value can be found even when the two poles have the same nature of anomaly; one pole is anomalously warmer (colder) than the other. More or less, ROM follows the event to event variability of anomaly pattern with some deficiency during 1982, when ROM shows a slight westward shifting negative anomaly pattern and warming over Bay of Bengal (BoB) rather than cooling reported observation. The inter–events variation of IOD is challenging for modeling. Even different reanalysis are also found to have significant variations in representing these inter-events characteristics of ocean temperature (Yang et al., 2020).

The IODE and IODW oppositely impact the climate of the region, including ISMR leading to the emergence of pseudo and actual dipoles. The similar(contrasting) nature of dipole structure for precipitation and SST is known as true(pseudo) IOD (Verdon-Kidd, 2018). Additionally, the spatially varying pattern of rainfall along with SSTA determines different IOD flavors (Verdon-Kidd, 2018). We computed the precipitation anomaly for all the IOD years (Fig. S4). The figure reveals the dipole structure with dry anomaly over the eastern pole and wet anomaly over the western pole. The stronger(weaker) anomalies are noticed during stronger(weaker) IOD years. Unlike SST composite in 2015, precipitation shows a clear dipole of dry and wet anomaly, indicating this year as pseudo-IOD years. ROM potentially distinguished the pseudo and true IOD years, which is challenging for most climate models (Doi et al., 2017).

3.2. Physical mechanism associated with IOD

The circulation features particularly the equatorial dynamics significantly impact the formation of IOD structure. Thus it is worthwhile to investigate the model's potential in simulating the governing mechanism. Fig. 5 depicts the prevailing easterly over eastern equatorial IO and southeasterly along the coast of Sumatra can be noticed during pIOD. This might favor the upwelling along the Sumatra, leading the region anomalously cold. This cold water advected over WEIO, enhancing the zonal surface gradient that further enhances the easterly and hence upwelling. The reverse is true for negative IOD years. The ROM correctly reproduces these features with some deficiency in its magnitude, particularity on the western IO, leading to a discrepancy in simulating the IOD. For example, the weaker wind over western EIO (WEIO) during pIOD reduces the warm water transport from the east pole to the western pole, leading to weaker warming on WEIO (5 N-5S).

Additionally, weaker northerly along Somalia might suppress the southward transport of warm water from the northern Arabian Sea (AS), leading to enhanced warming over western AS. Interestingly, during the apIOD, equatorial easterly wind split into two branches over the equatorial central Indian ocean (ECIO) rather than continuous flow from EEIO to WEIO in convention pIOD. The splitting of strong easterly from the EEIO into southward(northward) over CEIO suppresses the pile-up of water to the targeted region of conventional pIOD. It produces the weaker warm region over CEIO. ROM shows a deficiency in simulating the accurate representation of circulation pattern of low-level wind, mainly north-south divergent flow over CEIO, partially explaining the cause of weaker warming over in ROM over CEIO during apIOD. This might be associated with a noticeable deficiency in the upper-level wind, particularly equatorial westerly during nIOD years and equatorial easterly during pIOD and apIOD years. Additionally, the anticyclonic (cyclonic) circulation is found to be either shifted or very weak during negative(positive) IOD years (fig. S5).

Study by Ng et al. (2015) show that nonlinear processes such as, zonal advection, meridional advection, and entrainment play a vital role in determining the strength of IOD. Thus, it is worth diagnosing the model's potential in simulating these processes. It is noted that the zonal advection contributes substantially to the strength of the IOD (Fig. S6). The strength of zonal advection from the southeastern region shows covariability with the strength of pIOD. For example, during the extreme pIOD years 1997 (concurrent with ENSO year), the highest cold advection is noticed in the reanalysis. This is consistent with the previous study by Ng et al. (2015), who reported a more substantial advection during extreme pIOD year than the moderate pIOD. ROM shows reasonable skill in simulating the zonal advection during the weak and moderate pIOD year. Still, during the intense pIOD, the model significantly underestimates the cold advection, indicating the more prominent role of processes over the western pole in the model. A similar structure is observed for subsurface (at 50 m depth) zonal advection with slight differences in magnitude. Comparatively, a more significant discrepancy was noted for subsurface advection to the surface (fig. S7).

The more considerable (lesser) meridional advection was noticed during, the stronger(weaker) pIOD year, indicating its influence on pIOD strength (fig. S8). ROM shows reasonable skill in representing the spatial structure of the meridional advection structure for all the pIOD events. However, magnitudes are substantially differed with more substantial advection than reanalysis, particularly beyond 10^0S.

Apart from anomalous surface temperature variability, the subsurface temperature also varied substantially in response to IOD (Horii et al., 2008; Vinayachandran et al., 2002) which can be understood by investigating the thermocline variation. The vertical displacement of isotherm is tightly coupled to surface signals (Rao et al., 2002). The study by Ng et al. (2018) reported that thermocline depth (TCD) is one of the most responsive drivers of IOD variability. The deficiency in the model to simulate the mean TCD leads to diverging the IOD signal and generating significant variations in IOD amplitude. Thus it is vital to assess the model's ability in simulating the mean TCD and its propagation in the context of different phases of the IOD. Fig. 7 shows the longitude-depth variation of 26 °C isotherms (D26), which is used as the proxy for the middle of the thermocline and have potential *importance* for investigating the changes in the upper ocean because it is the depth to which the upper ocean heat content is integrated (Gera et al., 2013). The figure reveals the deepening of isotherm up to 100 m depth in the east and a slight rise over the west and central equatorial Indian Ocean during the negative phase of IOD. The reverse is true for pIOD. During apIOD, isotherm variability follows as the pIOD; however, rising(deepening) over eastern (central) EIO is more potent than during pIOD. ROM resembles observation in simulating this anomalous variability of isotherms during nIOD, pIOD, and apIOD with systematic differences in the magnitude of displacement. In general, a more considerable difference is noticed along the WEIO than EEIO during apIOD. The displacement of deepening (shoaling) of thermocline shifted the enhanced(suppressed) convection center, leading to intensifying the zonal gradient and the easterly wind, which further promotes the upwelling of Sumatra.

Further, the spatial distribution of the thermocline composite is analyzed (Fig. 8).The thermocline is defined as the 20^0 isothermal depth (D20). It is interesting to note that the D20 is found in the more deep ocean than 26^0 isothermal depth (D26).The figure reveals a dipole-like structure with moderate intensity over the conventional IOD region, with positive anomaly over the eastern and negative anomaly in the western poles during nIOD years and vice-versa during pIOD years. Besides, a stronger dipole over the southeastern Indian ocean (hereafter SIOD) has a positive anomaly along Sumatra and a negative anomaly along with southwest Sumatra during nIOD years and vice-versa during pIOD years. During apIOD, dipole structure is similar to pIOD with the difference in magnitude. This dipole is neither pure zonal nor meridional but shows southwest and northeast tilting. ROM reasonably reproduces the conventional IOD and SIOD with a systematic difference in magnitude and location. The deepening(shoaling) of the thermocline helps to sustain the warming(cooling) over the corresponding area, forces an anomalous wind towards the warm (cold) center in the lower(upper) troposphere (Fig. 5 and fig. S5). The shallow thermocline over the eastern pole of convention IOD in ROM, compared to observation during pIOD, leads to reduced warming and weakens equatorial easterly. Besides the positive thermocline anomaly of SIOD, it is confined over a smaller area with the southeastward shifting of its center and westward extension up to 65°E rather than the 50°E in observation, leading to shifting warming center and easterly from Sumatra. In general, the shoaling of the thermocline is noticed in RESM over the deeper region in

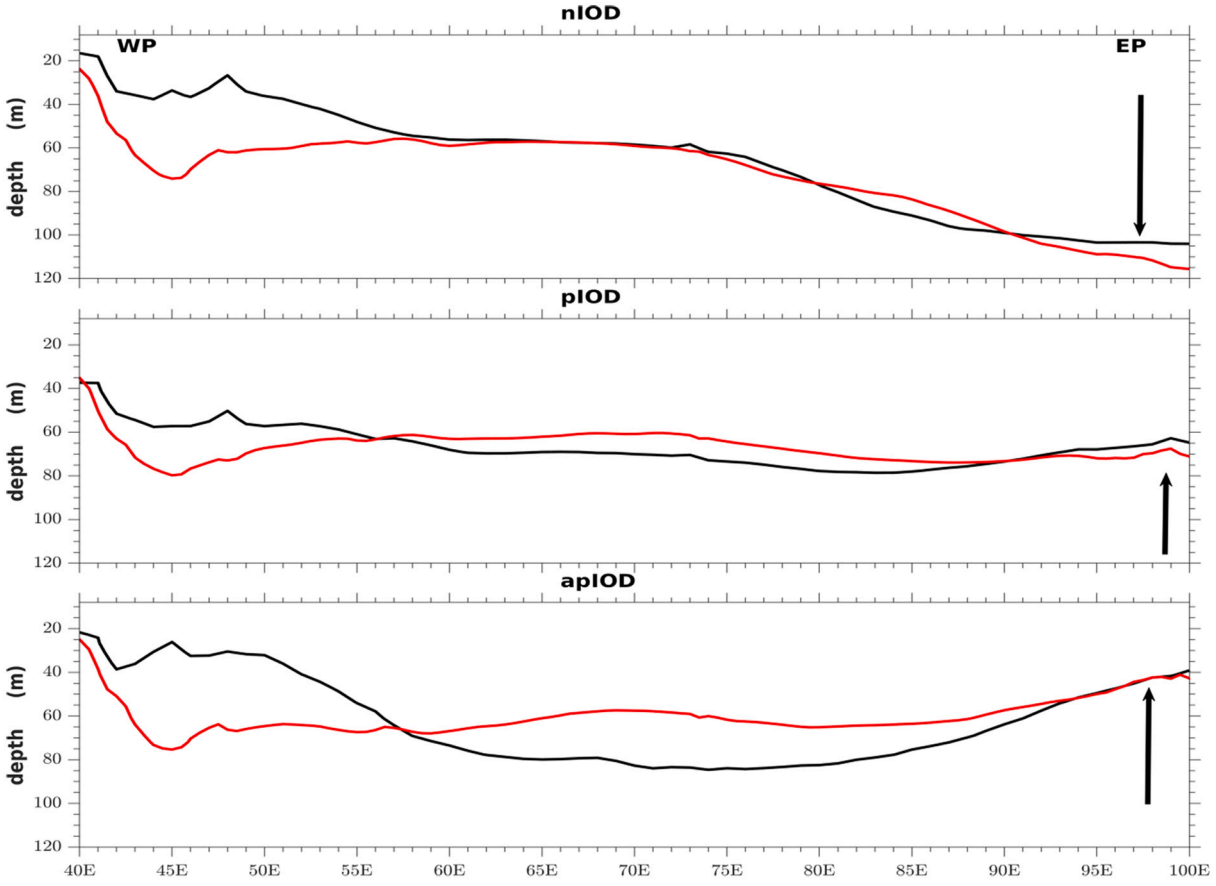

Fig. 7. Longitude depth variation of 26-degree isotherms (D26) averaged over the equatorial region (5S—5N). The solid black line is for observation, and red is for the model. WP and EP represent the western pole and eastern pole.The black arrow denotes the shallowing/deepening of mean D26. (For interpretation of the references to colour in this figure legend, the reader is referred to the web version of this article.)

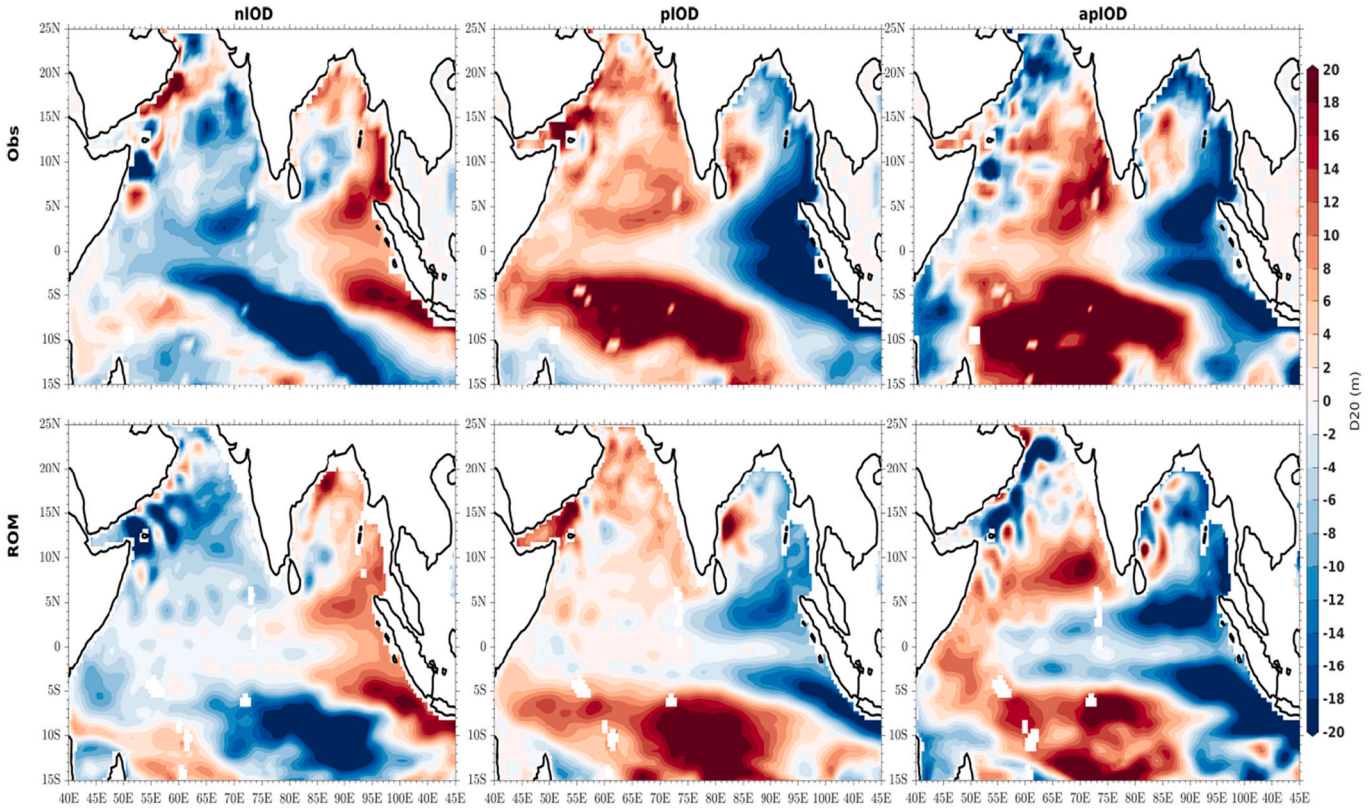

Fig. 8. Composite of the thermocline (D20) for nIOD, pIOD, and apIOD.

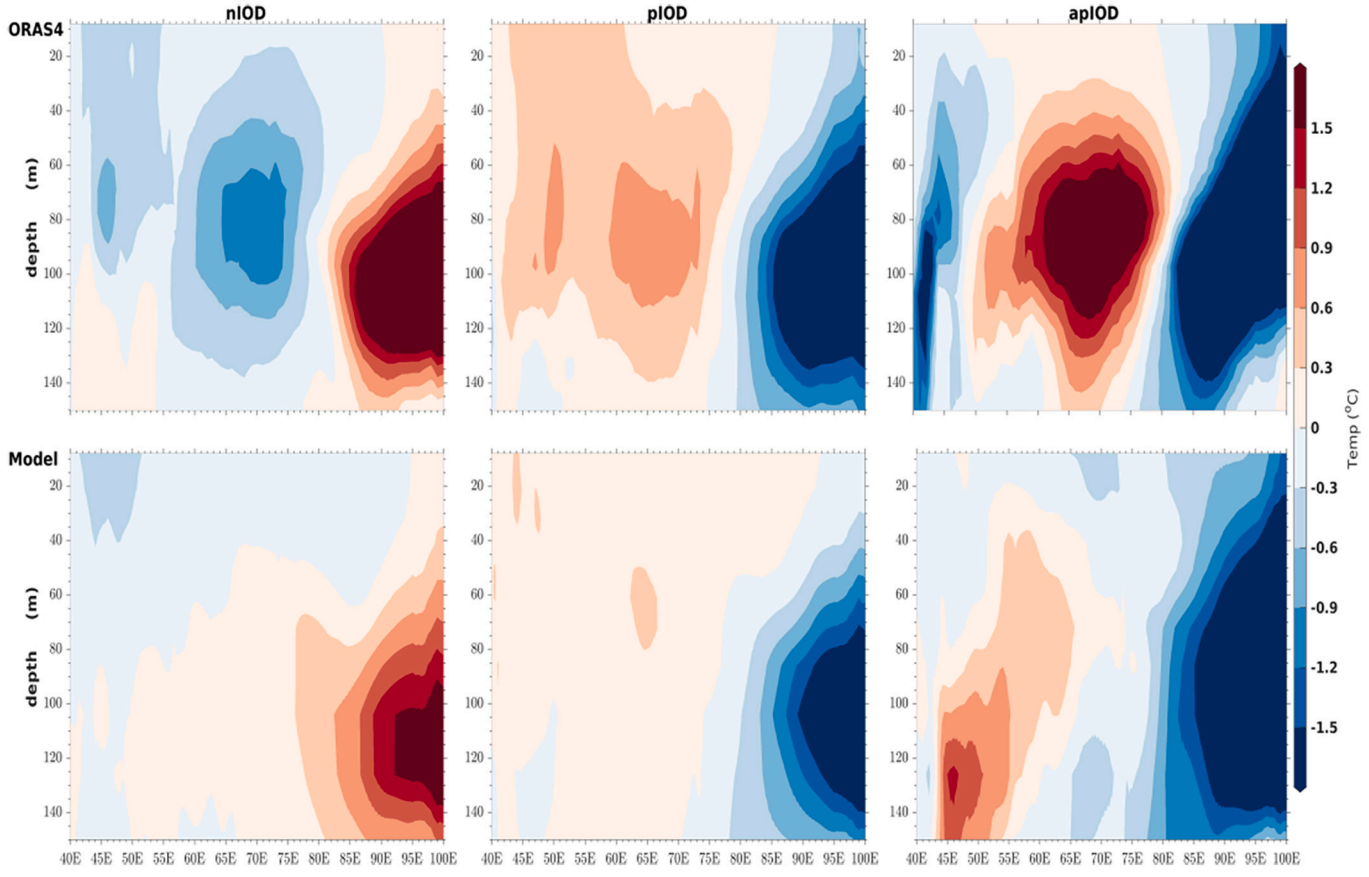

Fig. 9. Composite of subsurface equatorial temperature averaged over 5S to 5 N for nIOD, pIOD, and apIOD years.

observation.Additionally, shifting the equatorial deeper thermocline region of the central equatorial Indian ocean(CEIO) to the western equatorial Indian ocean (WEIO) leads to the shift in equatorial warming. This is associated with the southeasterly wind coming from Sumatra flows to the (WEIO) rather than converging to CEIO as in the case of observation. These facts indicate that the discrepancy in the subsurface process in the model leads to uncertainty in simulating the IOD.

The equatorial dynamics play a vital role in sustaining the favorable condition for IOD. The study by Rao et al. (2002) reported a strong connection between surface IOD and subsurface mode of variability (east-west dipole). We computed the subsurface temperature average composite over the equatorial region (5°S-5°N) for nIOD, pIOD, and apIOD years (Fig. 9). We observed a clear dipole structure in subsurface temperature with the warming of thermocline over eastern and cooling over western IO during nIODand vice-versa during pIOD. During apIOD, the structure of the eastern pole is similar to pIOD, but intensified and eastward shifting warm pole. ROM shows better skill in simulating subsurface temperature over the east pole. However, it shows a noticeable bias for the western pole consistent with the uncertainty in the surface dipole pattern of IOD. The warm thermocline water of the equatorial Indian Ocean is pushed towards the east, leading to the development of the warmer region of the east side. Further, its upwelling reduces the strength of the western cold pole in ROM compared to observation during nIOD. During pIOD, ROM shows lesser warming over

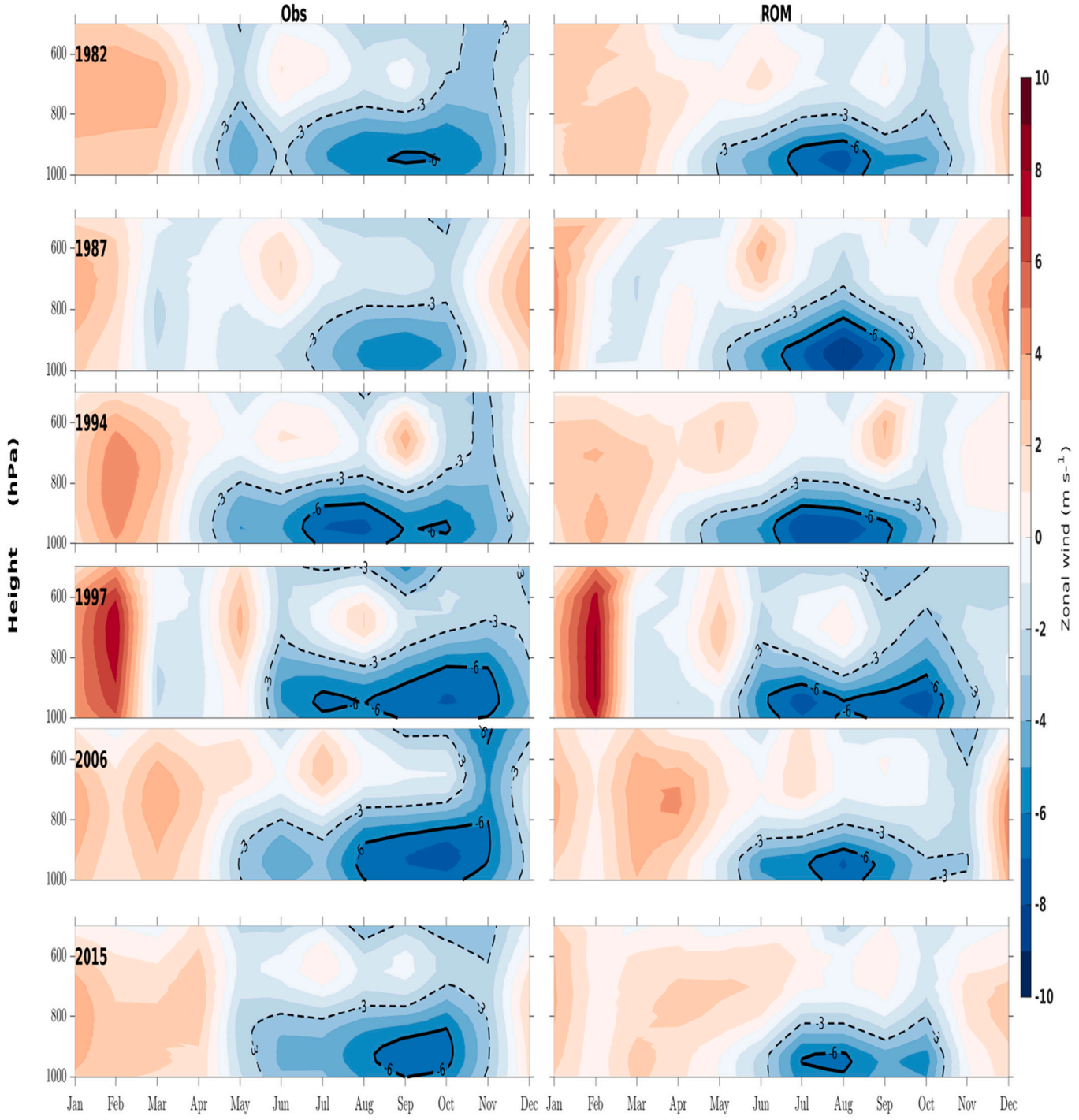

Fig. 10. Temporal evolution of zonal wind over the equatorial region (5S to 5 N) for different IOD events: first column for observation and second column for ROM.

western IO than observation, seen in surface structure, though its mechanism is not precise.

Similarly, the weakening of the strength of warm thermocline and contraction of its area and eastward shifting is noticed in ROM compared to observation. The surface cold water pushed up eastward, and further its downwelling leads to dilute the warm thermocline water. This difference is expected partly due to the difference in the horizontal and resolution. Additionally, bias over the western pole might be associated with the model deficiency in simulating the mesoscale process over the region around the great whirls pool (eddy dominant region), due to the coarse vertical resolution, particularly in the upper layer and simpler turbulence closure scheme of Pacanowski and Philander (1981) in MPIOM. This highlights the necessity of increasing the ocean model resolution (horizontal and vertical) of the model and deep investigation of the vertical mixing process together with improving the associated parameterization, which is beyond the scope of this study and remains the concern for future study.

The temporal evolution of equatorial zonal wind shows the substantial event-to-event variability in the time of the easterly establishment, its strength, and vertical extension (Fig. 10). The year of the early establishment of the maximum strength of low-level equatorial easterly wind is peculiar in terms of the earlier peak of IOD. ROM realistically simulates the temporal evolution and vertical extent of equatorial wind with a slight early peak and an overestimated easterly, consistent with an early peak of IOD.

The relevance of IOD amplitude simulation is also affected by the model's ability in simulating the ENSO due to the interaction of the ENSO-induced anomalous subsidence and IOD-induced anomalous convergence over the Bay of Bengal (Ashok et al., 2004). Thus it is worthwhile to investigate the model's potential in simulating ENSO. We computed the NINO3.4for ROM and corresponding observation of HadlSST (Fig. 11). The figure reveals that the model has the potential to distinguish the ENSO and non-ENSO years. ROM's simulated magnitude of the cold anomaly during La Niña years is comparable to observation, however, ROM overestimates the positive anomaly during El Niño. The more decisive El Niño years show a larger difference in model and observation. For example, in 1997; observation shows the development from May (having an anomaly of 0.75), attains its peak during December (having an anomaly of 2.37), and start diminishing afterward but continues the El Niño like anomaly up to March 1998 (having an anomaly of 1.02) (Table S2). ROM shows the early development from April (having an anomaly of 0.87), attains its peak during November (having an anomaly of 3.68), and starts diminishing afterward but continues the El Niño like anomaly up to March 1998 (having an anomaly of 0.68) (Table S1). These uncertainties might be partially related to weaker atmospheric teleconnection due to the absence of coupling beyond the South Asia region that could have attributed to the model's uncertainty in simulating IOD. Apart from this, we also estimated the ROM's potential in simulating the IOD-ENSO relationship. In this regard, we computed the correlation coefficient of IOD and NINO3.4 (Fig. S9). A lesser number of IODs appear to concur with ENSO in ROM than observation, indicating the more prominent occurrence of independent IOD in ROM than observation. This diminishes the relationship of IOD-ENSO having a correlation of 0.14 in ROM rather than 0.35 observation.

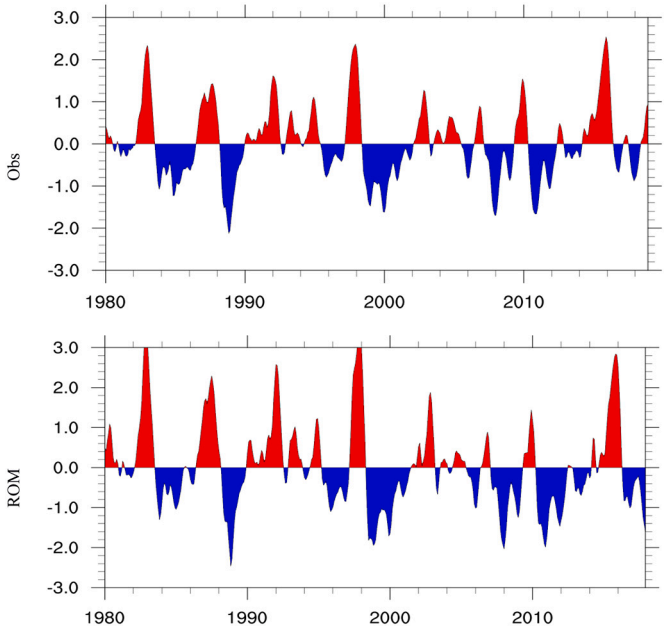

Fig. 11. NINO3.4 for ROM and observation.

The correct representation of IOD-ISMR is crucial for improving the monsoon rainfall projections. In general, most of GCMs display poor skills in representing the IOD-ISMR teleconnections. The changing relationship in the warming climate makes it challenging for the model to simulate ISMR correctly. Thus, it would be worth diagnosing the ROM's capability in representing the IOD-ISMR relationship. In this regard, we examine the relationship of IOD and ISMR in warming climate by computing the 21-years moving correlation between DMI and ISMR averaged over Indian land point for model and observation during JJAS (Fig. S10). From the figure, it can be noticed that the model shows a slightly different pattern of relationship during all decades. The misrepresentation of the ISMR–IOD relationship is one of the possible causes of model limitation in simulating the ISMR (overestimation over southwest-central India) reported in the earlier study of this model (Mishra et al., 2021a, 2021b). Most of the ISMR related studies have reported the limited skill of the model to reproduce ISMR correctly. However, investigating the cause of the failure and suggestions for improving them based on evidence would be more beneficial to the community because other researchers would be able to improve their models. In this regard, this study provides more space for minimising the model discrepancy and is scientifically helpful for the model community.

4. Conclusions

In this study, an effort is made to access the potential of a high-resolution regional earth system model (RESM), namely ROM, in simulating the Indian Ocean Dipole. In this regard, a simulation of thirty-eight years is carried out. It is observed that ROM realistically simulates the IOD phases (positive and negative), however, the magnitude of anomalies (warm and cold) shows some systematic discrepancy, particularly for the western pole. Despite the similar nature of anomaly at both poles, DMI can be observed as it is determined by relative SST anomaly differences, indicating that the existence of contrast anomaly over the eastern and western poles is not necessary for IOD events to occur. The model shows a varying skill for different flavors of IOD, highlights that only traditional(mean) IOD assessment is insufficient to prove the model reliability. We investigated how well the model simulates the different flavors of IOD that are vitally important for future climate change assessment. ROM shows a good resemblance in simulating the inter-event variability of the positive IOD's. The more decisive event is found to be dominated by significant cold anomalies over Sumatra with enhanced westward extension. However, a moderate event shows weakened cooling confined to the region of Sumatra. ROM has the potential to simulate the IOD amplitude with slight overestimation, which is a pervasive problem in most CMIP5/6 models reported in the earlier studies. However, overestimation in ROM is substantially less than the bias in the ensembles mean CMIP5 and CMIP6, indicating ROM's reliability towards the projection of the Indian summer monsoon. This overestimation of IOD amplitude might be partially attributed to the weaker IOD-ENSO relationship caused by the model tendency of producing a more significant number of IOD during

the non-ENSO year. Despite the proper representation of IOD characteristics, a slightly earlier peak of IOD driven by the early establishment of low-level equatorial easterly wind is observed. The shallow thermocline in the eastern Indian Ocean could lead to reduced thermal inertia, which causes the early peaking of the SST variability and higher values than in observations. This behavior of the thermocline could also lead to the early triggering of the easterlies, as the model has a stronger warm bias in the western than in the eastern equatorial regions. This study access the IOD's different phases and responsible forcings, limitations of the ROM in accounting for the role of internal climate variability that can be useful for further improvement in the model physics.

Data availability statement

The observational datasets used in this study are derived from public resources, and model data would be made available upon request to the corresponding author.

Author statement

Alok Kumar Mishra contributed to conceptualization, data curation, formal analysis, methodology, writing the original draft. Pankaj Kumar contributed to conceptualization, resources, funding acquisition, supervision, and writing, Aditya Kumar Dubey, contributed to data curation. Dimitry V. Sein contributed to model simulation. All authors have contributed to reviewing and editing the manuscript.

Declaration of Competing Interest

The authors declare that they have no known competing financial interests or personal relationships that could have influenced the work reported in this paper.

Acknowledgement

We thank the anonymous reviewers for their constructive comments and suggestions, which have helped us improve the overall quality of the paper. This work is jointly supported by the Department of Science and Technology (DST), Govt. of India, grant number DST/INT/RUS/RSF/P-33/G, and the Russian Science Foundation (Project No.: 19-47-02015). PK acknowledges funding from the Science and Engineering Research Board (SERB), Govt. of India grant number SB/S2/RJN-080/2014, and Department of Science and Technology (DST) grant number DST/CCP/NCM/69/2017(G). DS was supported in the framework of the state assignment of the Ministry of Science and Higher Education of Russia (theme No. 0128-2021-0014). The authors are thankful to the respective agencies of the IMD, ECMWF ERA-Interim, and HadISST data products for making these datasets available. Simulations were performed on the German Climate Computing Center (DKRZ) under the grant number ba1144. The authors declared that the manuscript contents are novel and neither published nor under consideration anywhere else. The authors also declared that they have no known financial interest.

Appendix A. Supplementary data

Supplementary data to this article can be found online at https://doi.org/10.1016/j.atmosres.2022.106182.

References

Ashok, K., Saji, N.H., 2007. On the impacts of ENSO and Indian Ocean dipole events on sub-regional Indian summer monsoon rainfall. Nat. Hazards 42, 273–285. https://doi.org/10.1007/s11069-006-9091-0.

Ashok, K., Guan, Z., Yamagata, T., 2001. Impact of the Indian Ocean dipole on the relationship between the Indian monsoon rainfall and ENSO. Geophys. Res. Lett. 28, 4499–4502. https://doi.org/10.1029/2001GL013294.

Ashok, K., Guan, Z., Yamagata, T., 2003. Influence of the Indian Ocean Dipole on the Australian winter rainfall. Geophys. Res. Lett. 30 https://doi.org/10.1029/2003GL017926.

Ashok, K., Guan, Z., Saji, N.H., Yamagata, T., 2004. Individual and combined influences of ENSO and the Indian Ocean Dipole on the Indian summer monsoon. J. Clim. 17, 3141–3155. https://doi.org/10.1175/1520-0442(2004)017<3141:IACIOE>2.0.CO;2.

Beck, H.E., Wood, E.F., Pan, M., Fisher, C.K., Miralles, D.G., Van Dijk, A.I.J.M., McVicar, T.R., Adler, R.F., 2019. MSWep v2 Global 3-hourly 0.1° precipitation: Methodology and quantitative assessment. Bull. Am. Meteorol. Soc. 100, 473–500. https://doi.org/10.1175/BAMS-D-17-0138.1.

Cai, W., Cowan, T., 2013. Why is the amplitude of the Indian Ocean Dipole overly large in CMIP3 and CMIP5 climate models? Geophys. Res. Lett. 40, 1200–1205. https://doi.org/10.1002/grl.50208.

Cai, W., Cowan, T., Raupach, M., 2009. Positive Indian Ocean Dipole events precondition Southeast Australia bushfires. Geophys. Res. Lett. 36, L19710. https://doi.org/10.1029/2009GL039902.

Cai, W., Zheng, X.T., Weller, E., Collins, M., Cowan, T., Lengaigne, M., Yu, W., Yamagata, T., 2013. Projected response of the Indian Ocean Dipole to greenhouse warming. Nat. Geosci. https://doi.org/10.1038/ngeo2009.

Cai, W., Santoso, A., Wang, G., Weller, E., Wu, L., Ashok, K., Masumoto, Y., Yamagata, T., 2014. Increased frequency of extreme Indian ocean dipole events due to greenhouse warming. Nature 510, 254–258. https://doi.org/10.1038/nature13327.

Cai, W., Yang, K., Wu, L., Huang, G., Santoso, A., Ng, B., Wang, G., Yamagata, T., 2021. Opposite response of strong and moderate positive Indian Ocean Dipole to global warming. Nat. Clim. Chang. 11, 27–32. https://doi.org/10.1038/s41558-020-00943-1.

Crétat, J., Terray, P., Masson, S., Sooraj, K.P., Roxy, M.K., 2017. Indian Ocean and Indian summer monsoon: relationships without ENSO in ocean–atmosphere coupled simulations. Clim. Dyn. 49, 1429–1448. https://doi.org/10.1007/s00382-016-3387-x.

Davies, H.C., 1976. A lateral boundary formulation for multi-level prediction models. Q. J. R. Meteorol. Soc. 102, 405–418. https://doi.org/10.1002/qj.49710243210.

Dee, D.P., Uppala, S.M., Simmons, A.J., Berrisford, P., Poli, P., Kobayashi, S., Andrae, U., Balmaseda, M.A., Balsamo, G., Bauer, P., Bechtold, P., Beljaars, A.C.M., van de Berg, L., Bidlot, J., Bormann, N., Delsol, C., Dragani, R., Fuentes, M., Geer, A.J., Haimberger, L., Healy, S.B., Hersbach, H., Hólm, E.V., Isaksen, L., Kållberg, P., Köhler, M., Matricardi, M., Mcnally, A.P., Monge-Sanz, B.M., Morcrette, J.J., Park, B. K., Peubey, C., de Rosnay, P., Tavolato, C., Thépaut, J.N., Vitart, F., 2011. The ERA-Interim reanalysis: Configuration and performance of the data assimilation system. Q. J. R. Meteorol. Soc. 137, 553–597. https://doi.org/10.1002/qj.828.

Di Sante, F., Coppola, E., Farneti, R., Giorgi, F., 2019. Indian Summer Monsoon as simulated by the regional earth system model RegCM-ES: the role of local air–sea interaction. Clim. Dyn. 53, 759–778. https://doi.org/10.1007/s00382-019-04612-8.

Doi, T., Storto, A., Behera, S.K., Navarra, A., Yamagata, T., 2017. Improved prediction of the Indian Ocean dipole mode by use of subsurface ocean observations. J. Clim. 30, 7953–7970. https://doi.org/10.1175/JCLI-D-16-0915.1.

Fan, L., Liu, Q., Wang, C., Guo, F., 2017. Indian ocean dipole modes associated with different types of ENSO development. J. Clim. 30, 2233–2249. https://doi.org/10.1175/JCLI-D-16-0426.1.

Giorgi, F., Jones, C., Asrar, G., 2009. Addressing climate information needs at the regional level: the CORDEX framework. World Meteorological Organization (WMO) Bullet. 58 (3), 175.

Griffies, S.M., 1998. The Gent-McWilliams skew flux. J. Phys. Oceanogr. 28, 831–841. https://doi.org/10.1175/1520-0485(1998)028<0831:TGMSF>2.0.CO;2.

Hagemann, S., Dümenil, L., 1998. A parametrization of the lateral waterflow for the global scale. Clim. Dyn. https://doi.org/10.1007/s003820050205.

Hong, C.-C., Lu, M.-M., Kanamitsu, M., 2008. Temporal and spatial characteristics of positive and negative Indian Ocean dipole with and without ENSO. J. Geophys. Res. 113, D08107. https://doi.org/10.1029/2007JD009151.

Horii, T., Hase, H., Ueki, I., Masumoto, Y., 2008. Oceanic precondition and evolution of the 2006 Indian Ocean dipole. Geophys. Res. Lett. 35, L03607. https://doi.org/10.1029/2007GL032464.

Hrudya, P.P.V.H., Varikoden, H., Vishnu, R.N., 2021. Changes in the relationship between Indian Ocean dipole and Indian summer monsoon rainfall in early and recent multidecadal epochs during different phases of monsoon. Int. J. Climatol. 41, E305–E318. https://doi.org/10.1002/joc.6685.

Jacob, D., 2001. A note to the simulation of the annual and inter-annual variability of the water budget over the Baltic Sea drainage basin. Meteorog. Atmos. Phys. 77, 61–73. https://doi.org/10.1007/s007030170017.

Jungclaus, J.H., Fischer, N., Haak, H., Lohmann, K., Marotzke, J., Matei, D., Mikolajewicz, U., Notz, D., Storch, J.S., 2013. Characteristics of the ocean simulations in the Max Planck Institute Ocean Model (MPIOM) the ocean component of the MPI-Earth system model. J. Adv. Model. Earth Syst. 5, 422–446. https://doi.org/10.1002/jame.20023.

Mahto, S.S., Mishra, V., 2019. Does ERA-5 Outperform Other Reanalysis Products for Hydrologic applications in India? J. Geophys. Res. Atmos. 124, 9423–9441. https://doi.org/10.1029/2019JD031155.

Marsland, S.J., Haak, H., Jungclaus, J.H., Latif, M., Röske, F., 2002. The Max-Planck-Institute global ocean/sea ice model with orthogonal curvilinear coordinates. Ocean Model 5, 91–127. https://doi.org/10.1016/S1463-5003(02)00015-X.

McKenna, S., Santoso, A., Gupta, A. Sen, Taschetto, A.S., Cai, W., 2020. Indian Ocean Dipole in CMIP5 and CMIP6: characteristics, biases, and links to ENSO. Sci. Rep. 10, 11500. https://doi.org/10.1038/s41598-020-68268-9.

Mishra, A.K., Dwivedi, S., Di Sante, F., 2021a. Performance of the RegCM-MITgcm coupled Regional Model in Simulating the Indian Summer Monsoon Rainfall. Pure Appl. Geophys. https://doi.org/10.1007/s00024-020-02648-0.

Mishra, A.K., Kumar, P., Dubey, A.K., Javed, A., Saharwardi, M.S., Sein, D.V., Martyanov, S.D., Jacob, D., 2021b. Impact of horizontal resolution on monsoon precipitation for CORDEX-South Asia: a regional earth system model assessment. Atmos. Res. 259, 105681 https://doi.org/10.1016/j.atmosres.2021.105681.

Ng, B., Cai, W., Walsh, K., Santoso, A., 2015. Nonlinear processes reinforce extreme Indian Ocean Dipole events. Sci. Rep. 5, 1–10. https://doi.org/10.1038/srep11697.

Ng, B., Cai, W., Cowan, T., Bi, D., 2018. Influence of internal climate variability on Indian Ocean Dipole properties. Sci. Rep. 8, 1–8. https://doi.org/10.1038/s41598-018-31842-3.

Pokhrel, S., Chaudhari, H.S., Saha, S.K., Dhakate, A., Yadav, R.K., Salunke, K., Mahapatra, S., Rao, S.A., 2012. ENSO, IOD and Indian Summer Monsoon in NCEP climate forecast system. Clim. Dyn. 39, 2143–2165. https://doi.org/10.1007/s00382-012-1349-5.

Rao, S.A., Behera, S.K., Masumoto, Y., Yamagata, T., 2002. Interannual subsurface variability in the tropical Indian Ocean with a special emphasis on the Indian Ocean Dipole. Deep. Res. Part II Top. Stud. Oceanogr. 49, 1549–1572. https://doi.org/10.1016/S0967-0645(01)00158-8.

Rayner, N.A., Parker, D.E., Horton, E.B., Folland, C.K., Alexander, L.V., Rowell, D.P., Kent, E.C., Kaplan, A., 2003. Global analyses of sea surface temperature, sea ice, and night marine air temperature since the late nineteenth century. J. Geophys. Res. Atmos. 108 https://doi.org/10.1029/2002jd002670.

Rechid, D., Raddatz, T.J., Jacob, D., 2009. Parameterization of snow-free land surface albedo as a function of vegetation phenology based on MODIS data and applied in climate modelling. Theor. Appl. Climatol. 95, 245–255. https://doi.org/10.1007/s00704-008-0003-y.

Reynolds, R.W., Smith, T.M., Liu, C., Chelton, D.B., Casey, K.S., Schlax, M.G., 2007. Daily high-resolution-blended analyses for sea surface temperature. J. Clim. https://doi.org/10.1175/2007JCLI1824.1.

Saji, N., Yamagata, T., 2003. Possible impacts of Indian Ocean Dipole mode events on global climate. Clim. Res. 25, 151–169. https://doi.org/10.3354/cr025151.

Saji, N.H., Goswami, B.N., Vinayachandran, P.N., Yamagata, T., 1999. A dipole mode in the tropical Indian ocean. Nature 401, 360–363. https://doi.org/10.1038/43854.

Sein, D.V., Mikolajewicz, U., Gröger, M., Fast, I., Cabos, W., Pinto, J.G., Hagemann, S., Semmler, T., Izquierdo, A., Jacob, D., 2015. Regionally coupled atmosphere-ocean-sea ice-marine biogeochemistry model ROM: 1. Description and validation. J. Adv. Model. Earth Syst. 7, 268–304. https://doi.org/10.1002/2014MS000357.

Sein, D.V., Gröger, M., Cabos, W., Alvarez-Garcia, F.J., Hagemann, S., Pinto, J.G., Izquierdo, A., de la Vara, A., Koldunov, N.V., Dvornikov, A.Y., Limareva, N., Alekseeva, E., Martinez-Lopez, B., Jacob, D., 2020. Regionally coupled Atmosphere-Ocean-Marine Biogeochemistry Model ROM: 2. Studying the climate Change Signal in the North Atlantic and Europe. J. Adv. Model. Earth Syst. https://doi.org/10.1029/2019MS001646.

Steele, M., Morley, R., Ermold, W., 2001. PHC: a global ocean hydrography with a high-quality Arctic Ocean. J. Clim. https://doi.org/10.1175/1520-0442(2001)014<2079:PAGOHW>2.0.CO;2.

Sun, S., Fang, Y., Tana, Liu, B., 2014. Dynamical mechanisms for asymmetric SSTA patterns associated with some Indian Ocean Dipoles. J. Geophys. Res. Oceans. 119, 3076–3097.

Sun, S., Lan, J., Yue Fang, T., Gao, X., 2015. A triggering mechanism for the Indian Ocean dipoles independent of ENSO. J. Clim. 28, 5063–5076. https://doi.org/10.1175/JCLI-D-14-00580.1.

Thomas, M., Sündermann, J., Maier-Reimer, E., 2001. Consideration of ocean tides in an OGCM and impacts on subseasonal to decadal polar motion excitation. Geophys. Res. Lett. https://doi.org/10.1029/2000GL012234.

Ummenhofer, C.C., England, M.H., McIntosh, P.C., Meyers, G.A., Pook, M.J., Risbey, J.S., Gupta, A. Sen, Taschetto, A.S., 2009. What causes Southeast Australia's worst droughts? Geophys. Res. Lett. 36, L04706. https://doi.org/10.1029/2008GL036801.

Valcke, S., 2013. The OASIS3 coupler: a European climate modelling community software. Geosci. Model Dev. 6, 373–388. https://doi.org/10.5194/gmd-6-373-2013.

Verdon, D.C., Franks, S.W., 2005. Indian Ocean Sea surface temperature variability and winter rainfall: Eastern Australia. Water Resour. Res. 41, 1–10. https://doi.org/10.1029/2004WR003845.

Verdon-Kidd, D.C., 2018. On the classification of different flavours of Indian Ocean Dipole events. Int. J. Climatol. 38, 4924–4937. https://doi.org/10.1002/joc.5707.

Vinayachandran, P.N., Iizuka, S., Yamagata, T., 2002. Indian Ocean dipole mode events in an ocean general circulation model. Deep. Res. Part II Top. Stud. Oceanogr. 49, 1573–1596. https://doi.org/10.1016/S0967-0645(01)00157-6.

Wang, B., Xiang, B., Li, J., Webster, P.J., Rajeevan, M.N., Liu, J., Ha, K.J., 2015. Rethinking Indian monsoon rainfall prediction in the context of recent global warming. Nat. Commun. 6 https://doi.org/10.1038/ncomms8154.

Yang, K., Cai, W., Huang, G., Wang, G., Ng, B., Li, S., 2020. Oceanic Processes in Ocean Temperature Products Key to a Realistic Presentation of positive Indian Ocean Dipole Nonlinearity. Geophys. Res. Lett. 47 https://doi.org/10.1029/2020GL089396 e2020GL089396.

Zuo, H., Balmaseda, M.A., Tietsche, S., Mogensen, K., Mayer, M., 2019. The ECMWF operational ensemble reanalysis-analysis system for ocean and sea ice: a description of the system and assessment. Ocean Sci. 15, 779–808. https://doi.org/10.5194/os-15-779-2019.

Pacanowski, R.C., Philander, S.G.H., 1981. Parameterization of vertical mixing in numerical models of tropical cceans. J. Phys. Oceanogr. 11, 1443–1451. https://doi.org/10.1175/1520-0485(1981)011<1443:POVMIN>2.0.CO;2.